

THESIS FOR THE DEGREE OF LICENCIATE OF PHILOSOPHY

Studies of Charge Separation in Molecular and Molecular-Inorganic materials Assemblies for Solar Energy Conversion

Valeria Saavedra Becerril



CHALMERS
UNIVERSITY OF TECHNOLOGY

Department of Chemistry and Chemical Engineering
Chalmers University of Technology
Göteborg, Sweden
2015

Studies of Charge Separation in Molecular and Molecular-Inorganic materials
Assemblies for Solar Energy Conversion
Valeria Saavedra Becerril

© Valeria Saavedra Becerril, 2015

Chalmers Tekniska Högskola

Licuppsatser vid Institutionen för kemi och kemiteknik. 2015:05

ISSN nr: 1652-943X

Department of Chemistry and Chemical Engineering

Chalmers University of Technology

SE-41296 Gothenburg

Sweden

Telephone +46(0) 31 772 1000

Cover picture: Principles of artificial photosynthesis for solar fuel production from water. D = donor, P = photosensitizer unit, A = acceptor.

Chalmers Reproservice

Göteborg, Sweden 2015

List of Publications

This thesis is based on the following publication and manuscript:

- I. Karlsson, E. A.; Lee, B-L.; Liao, R-Z.; Åkermark, T.; Kärkäs, M. D.; Saavedra Becerril, V.; Siegbahn, P. E. M.; Zou, X.; Abrahamsson, M.; Åkermark, B. *Synthesis and Electron-Transfer Processes in a New Family of Ligands for Coupled Ru-Mn₂ Complexes*. Published in *ChemPlusChem*.
- II. Saavedra Becerril, V. Franchi, D. Abrahamsson, M. *Back electron transfer kinetics in D35-sensitized TiO₂ in ionic liquid electrolytes: effect of ionic liquid composition*. Manuscript in preparation.

CONTRIBUTION REPORT

- I. Performed all steady-state and time-resolved emission experiments and wrote part of the manuscript.
- II. Suggested the project, planned and performed all the experiments, and wrote the manuscript.

Abstract

Conversion of solar energy and its storage in the form of chemical bonds is a current scientific and technological challenge. Different approaches to achieve light-harvesting followed by efficient charge separation are the focus on this thesis. This includes purely molecular approaches inspired by natural photosynthesis, and hybrid molecular-inorganic material (hybrid) approaches where the functions of both, molecules and solid materials are combined to obtain desired long-lived charge separation. The long-term goal is to create an assembly that is able to efficiently produce solar fuel.

The study of excited state reactions such as photoinduced electron transfer is crucial for the understanding of solar energy conversion systems. In this thesis, electron-transfer processes in one molecular and one hybrid assembly were studied.

In the molecular approach, a series of $[\text{Ru}(\text{bpy})_3]^{2+}$ -type photosensitizers have been covalently attached to a dinuclear Mn_2 -ligand that has previously shown photocatalytic water oxidation activity in bimolecular reactions. However, upon integrating photosensitizer and catalyst into one structure, water oxidation activity was shut off. Detailed investigation of the photophysical properties revealed unusually short-lived and strongly pH-dependent excited state decay patterns. The major contribution to the observed short lifetimes was presumably an electron-transfer quenching process originating from the ligand connecting the ruthenium and manganese centers.

The hybrid assembly consisted of dye-sensitized mesoporous TiO_2 nanoparticles, using the organic dye D35. The efficiency of this type of systems depends, to a great extent, on the kinetics of interfacial electron-transfer processes. Here, photoinduced back electron transfer, an efficiency limiting process, was investigated in the presence of ionic liquid (IL) electrolytes. The aim was to be able to reduce the rate of back electron transfer by taking advantage of the structural properties of the ionic liquids. It was hypothesized that cations accumulated at the TiO_2 surface, could temporarily interfere with the recombination of the dye with the electrons in the conduction band of TiO_2 . Transient absorption measurements show that the kinetics of back electron transfer decreased in the presence of 1-butyl- and 1-hexyl-3-methylimidazolium hexafluorophosphate ILs (14000 and 7000 s^{-1} respectively) compared to that in organic solvent based electrolytes (24000 in CH_3CN and 41000 s^{-1} in $\text{CH}_3\text{CN}/\text{LiClO}_4$). In conclusion, the bulkier the cations, the longer the lifetime of the charge separated state.

Keywords: solar fuel, water oxidation, charge-separation, photoinduced electron transfer, dye-sensitized.

Table of Contents

1. Introduction	1
2. Theory	3
2.1 Thermodynamics and kinetics	3
2.2 Energy levels of molecules	5
2.3 Light-matter interactions: <i>photophysics</i>	7
2.4 Excited state reactions	10
2.4.1 Energy transfer	10
2.4.2 Photoinduced electron transfer	10
2.4.3 Interfacial electron transfer: <i>Semiconductor-dye interactions</i>	12
3. Approaches to solar energy conversion for fuel production	15
3.1 Molecular approaches	15
3.2 Inorganic materials approaches	16
3.3 Hybrid molecular-inorganic materials assemblies	17
4. Experimental techniques	19
4.1 Electrochemical methods	19
4.1.1 Cyclic voltammetry	19
4.1.2 Differential pulse voltammetry (DPV)	19
4.1.3 Bulk electrolysis methods	20
4.2 Optical spectroscopy methods	20
4.2.1 Steady state absorption spectroscopy	20
4.2.2 Nanosecond-transient absorption spectroscopy	21
4.2.3 Steady-state emission spectroscopy	22
4.2.4 Time correlated single photon counting (TCSPC)	23
4.3 Spectroelectrochemistry	24
5. Results and discussion	25
5.1 Molecular approach to photocatalytic water oxidation: a Ru-Mn ₂ model complex	25
5.1.1 Electrochemical characterization	27
5.1.2 Photophysical characterization: absorption and emission properties	27
5.1.3 Undesired excited state reactions explain the unsuccessful water oxidation	30
5.2 Interfacial electron transfer in dye-sensitized TiO₂ nanoparticles	31
5.2.1 Description of the molecular-inorganic material assembly	32
5.2.2 The use of ionic liquids to control back-electron transfer	33
6. Summary and future perspective	38
Acknowledgments	38
References	39

List of abbreviations

(CO ₂ Et) ₂ bpy	Diethylester bipyridine
[Ru(bpy) ₃] ²⁺	Tris(2,2'-bipyridine)ruthenium(II) ion
A	Acceptor
BMIMI	1-Butyl-3-methylimidazolium iodide
BMIMPF ₆	1-Butyl-3-methylimidazolium hexafluorophosphate
BMIMSCN	1-Butyl-3-methylimidazolium thiocyanate
CB	Conduction band
CBM	Conduction band mediated
CCD	Charge coupled device
CE	Counter electrode
CV	Cyclic voltametry
D	Donor
DFT	Density functional theory
DPV	Differential pulse voltametry
DSSC	Dye-sensitized solar cells
GS	Ground state
HMIMPF ₆	1-hexyl-3-methylimidazolium hexafluorophosphate
HOMO	Highest occupied molecular orbital
IC	Internal conversion
IL	Ionic liquids
IRF	Instrument response function
ISC	Intersystem crossing
LUMO	Lowest unoccupied molecular orbital
MLCT	Metal-to-ligand charge transfer
MO	Molecular orbital
NHE	Normal hydrogen electrode
OEC	Oxygen-evolving complex
PET	Photoinduced electron transfer
RE	Reference electrode
TAC	Time to amplitude converter
TCSPC	Time correlated single photon counting
UV	Ultraviolet
VB	Valence band
WE	Working electrode
ΔA	Differential absorption

1. Introduction

Concerns about the climate and future of the Earth are constantly increasing since there is a clear consensus among scientists on the direct relation between human activities, incremented greenhouse gas emissions and the global warming and its manifestations.^{1,2} It is estimated that about 97% of the climate researchers agree that the causes of climate changes are anthropogenic.²

The majority of greenhouse emissions primarily originate from coal-fired power plants, transportation and industry.³ Currently, 81% of the total primary energy supply is generated from fossil fuels only 1.7% from other renewable sources such as solar and wind.⁴ Consequently, a challenge of our time is to replace the use of fossil fuels with other forms of clean and renewable sources to considerably decrease greenhouse emissions.

Although renewable sources already provide about 10% of the world energy consumption, currently, none of them could fully replace fossil fuel technologies alone, and therefore a combination of solutions is more likely to be the answer. However, there is one source that contains so much energy, that in one hour, could provide the earth with the total power consumed by humans in one year: the sun.⁵ On top of that, solar energy can be used in safe, clean and sustainable manners. Efficient devices for using solar energy to either produce heat or electricity are already commercially available, however the importance of finding efficient and low-cost methods for storing it must be highlighted, owing to the fact that the suitability of harvesting solar energy is variable in the various regions of the earth.

The development of solar energy technology has been possible thanks to the observation of the photoelectric effect by Alexandre Becquerel in the mid-19th century.⁶ Ever since then, the idea of converting light into electricity or chemical fuels has been fascinating to scientists, and much effort has been dedicated to achieve this goal.

Direct storage of solar energy in the form of chemical bonds is a strategy that nature has perfected during billions of years of evolution. In photosynthesis, the energy from the sun is used to create fuel in the form of carbohydrates from water and carbon dioxide; impressive molecular machines transform the energy from photons into chemical energy. Several chemical approaches to the production of solar fuels have been studied. These are mainly intended to produce hydrogen from water^{7,8} and methane or methanol from carbon dioxide.^{9,10} Special attention has been given to the creation of a synthetic, photochemical system that converts solar energy into a storable fuel, using the principles of natural photosynthesis.¹¹

A significant challenge with production of solar fuels is to accumulate multiple redox equivalents, in systems where only single photon absorption processes take place. A molecular approach could solve this problem but the difficulty of synthesizing stable molecules, capable of multiple charge separation events, leads to the necessity to find other strategies.¹⁰ One of them is to combine molecular light harvesters and selective catalysts with materials that have

good charge carrier and electron storage properties such as semiconductors. Although this offers greater stability and control over the system components, other challenges arise, such as understanding and controlling the complex interfacial properties and physical-chemical processes in these assemblies.

This thesis concerns the study of key electron transfer processes in one molecular and one molecular-inorganic material assembly for solar energy conversion. In the first work, a series of photosensitizers were designed to be integrated to a manganese catalyst to obtain an assembly able to perform photochemical oxidation of water. Because this process was not successful, the photophysical properties of the photosensitizers, their precursors, and the photosensitizer-catalyst assembly were investigated in detail. Steady-state and time-resolved spectroscopic techniques, where used to reveal the possible mechanisms that interfered with the splitting of water. In the second work, a molecular-inorganic material assembly, where a photosensitizer was attached to semiconductor nanoparticles was studied. The effect of surrounding electrolytes on one efficiency limiting process to solar conversion was studied by time-resolved spectroscopy. The aim here was to achieve longer-lived charge separation states in dye-semiconductor assemblies, a crucial requirement for efficient solar energy conversion.

A conclusive remark from the comparison of these studies is that purely molecular strategies for the conversion and storage of solar energy, are much more challenging in the sense that the electronic processes in complex molecules are harder to control than in hybrid organic-inorganic material assemblies. Despite the advantages of molecular design, this tool seems to be insufficient to obtain all the properties needed in a solar energy conversion assembly. Consequently, I emphasize that a large part of the efforts toward functional assemblies for solar energy conversion and storage, must be directed toward the effective integration of molecular and inorganic materials.

2. Theory

This chapter is intended to introduce essential concepts and theories of thermodynamics, kinetics and photophysics which are related to the work presented in this thesis.

2.1 Thermodynamics and kinetics

Thermodynamics is the study of the transformations of energy, that is, the capacity of a system to do work.¹⁷ Thermodynamics is useful to determine if a chemical reaction will spontaneously occur. The initial and final equilibrium states of a system have energy properties that can be related to the direction and extent of a reaction. The Gibbs free energy is a very important thermodynamic property. For a chemical reaction to spontaneously occur the change in Gibbs free energy, ΔG , must be negative. This means that the energy of the products has to be lower than that of the reactants. The larger this difference the greater the driving force for the reaction to occur. The following equation represents the change in Gibbs free energy at constant temperature and pressure:

$$\Delta G_{T,P} = \Delta H - T\Delta S \quad (2.1)$$

where ΔH is the change in enthalpy, T is the temperature and ΔS is the entropy change.

Thermodynamics is useful to predict the direction and spontaneity of a chemical process, however, in most cases, thermodynamics do not influence how fast the reactants are converted into products, in other words, it is blind to what happens between the initial and final states (transitory states). There are however exceptions where thermodynamics actually control the speed of reactions, such as in the case of some electron transfer reactions which will be discussed in section 2.4.

Measurable properties related to the Gibbs free energy are used to predict the direction of reactions, for example, in electrochemical reactions, where electrons are transferred between chemical entities, the electric potential difference that develops when two conducting phases are brought into contact can be measured.¹² The simplest electrochemical system to describe is the galvanic cell, in which chemical energy is converted into electrical energy by oxidation-reduction (redox) reactions. The interesting property here is the electrical work, which is related to the change of the Gibbs free energy as follows:

$$\Delta G_{T,P} = -nFE \quad (2.2)$$

where n is the number of moles of electrons transferred, F is the Faraday constant and E is the potential difference; the negative sign implies that the system transfers energy to its surroundings rather than work being done on the system.¹² The Gibbs free energy of a redox reaction, can be calculated from the Nernst equation (2.3), a new property called the standard

potential is introduced by defining $E^\circ = \Delta G^\circ/nF$. For a cell operating at 25°C, the Nernst equation is written as follows:

$$E = E^\circ - \frac{0.0592}{n} \log \frac{[C]^c [D]^d}{[A]^a [B]^b} \quad (2.3)$$

where the logarithmic fraction represents the quotient of the product's and reactant's activities of the redox reaction: $aA + bB \leftrightarrow cC + dD$. The standard potentials are used to predict if an electrochemical reaction will spontaneously occur.

Kinetics, from the greek "kinesis" means movement or to move. Chemical kinetics is concerned with the study of the rate of reactions, which depends on the energy barriers existing between the initial and final states.¹³ Kinetics is about reactivity and it is also devoted to the study of the reaction mechanisms.

The origins of chemical kinetics date back to the XIX century when the first empirical observations of the influence of the temperature on the rate of a reaction were made¹⁴ and with the works of Jacobus van 't Hoff and Svante Arrhenius* who mathematically described the relationship between temperature and the rate of chemical reactions^{15,16}, as represented in the following equation:^{17,18}

$$k = Ae^{-E_a/(RT)} \quad (2.4)$$

Where k is the reaction rate constant, A is the frequency factor, which measures the rate of collisions, E_a is the activation energy, T is the temperature and R is the universal gas constant.

The most important concept of kinetics, the activation energy, E_a , represents the height of the energy barrier that separates the products from the reactants (Figure 2.1). This kinetic energy is the minimum input energy required to transform the reactants into products. This energy could be in the form of heat, light or electricity.

* Svante August Arrhenius (1859-1927) was a Swedish physicist that made important contributions to the field of chemistry including his theory on ionic dissociation of electrolytes, for which he received the Chemistry Nobel Prize in 1903.¹⁷ He was even the first scientist to propose that the change in carbon dioxide concentration in the atmosphere could affect the Earth's surface temperature.²¹

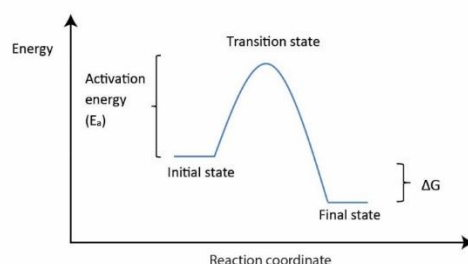


Figure 2.1. Schematic representation of the activation energy in relation to the energy of the final and initial states of a chemical system.

2.2 Energy levels of molecules.

When it comes to the description of chemical systems, quantum mechanics is essential, since classical mechanics fails to fully explain the physical phenomena at the atomic and sub-atomic scale. Quantum mechanics is used to properly describe the dual behavior (wave-particle) of elementary particles and to explain light-matter interactions. The description of the wave-like behavior of electrons in an atom is given by wave functions known as atomic orbitals. These functions are obtained by solving the time independent Schrödinger equation:

$$H\varphi = E\varphi \quad (2.5)$$

where φ is a wave function (molecular orbital) in stationary state and E is the corresponding eigenvalue, in this case the energy of the state φ . The values that φ can take are quantized** and they represent the distribution of the electron in the atom,¹⁷ that is, the probability of finding an electron at a certain position relative to the nuclei. The H operator corresponds to the total energy of the system (kinetic and potential), described by the Hamiltonian operator, which for n number of particles can be written as follows:

$$\hat{H} = -\frac{\hbar^2}{2} \sum_{n=1}^N \frac{1}{m_n} \nabla_n^2 + V(r_1, r_2 \dots r_n, t) \quad (2.6)$$

where r_n represents the interparticle distances and m_n is the mass of the particles. By linear combination of the atomic wave functions, molecular orbitals (MOs) can be constructed. However, solving the Schrödinger equation for polyatomic molecules is a complex mathematical problem that gets much simpler by introducing the *Born-Oppenheimer approximation*. This approximation is derived from the great difference between the masses of the nuclei and electrons. Based on this, the assumption that during an electronic transition the

** Restricted to a discrete set of values

nuclei has fixed spatial coordinates is valid. This results in decoupling of the motion of electrons from that of nuclei. Under this approximation the total wavefunction of a molecule can be written as:²⁰

$$\varphi_{total} = \varphi_{electronic}\varphi_{nuclear} \quad (2.7)$$

The spatial shape of the electronic wave functions is given by the probability density $|\varphi^2|$. By taking its absolute value, a delimited region where the probability density is constant can be computed. Electrons will fill the orbitals starting with the lowest energy level before occupying higher levels (Aufbau-principle), see Figure 2.2.

Orbitals with the same energy are referred to as degenerate, and they can differ from each other by their multiplicity, which is defined as $2S+1$, where S is the angular spin^{***} momentum. According to *Pauli's exclusion principle*, two electrons occupying the same orbital must have opposite spins and following *Hund's rule*, if several degenerated orbitals are available, the electrons will occupy them singly first instead of in pairs. Accordingly, the more unpaired electrons the larger the multiplicity. A state with all electrons paired is called a singlet state (S) and a state with two unpaired electrons is called a triplet (T). Ground states are typically singlets, but there are some exceptions such as molecular oxygen whose ground state is a triplet.

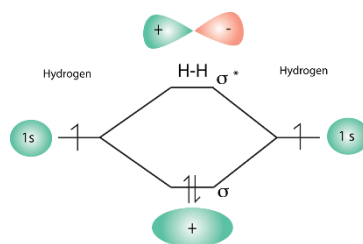


Figure 2.2 Molecular orbitals in the hydrogen molecule showing the sigma bonding orbital σ and the sigma anti-bonding orbital σ^* .

The highest occupied orbital (HOMO) and lowest unoccupied molecular orbital (LUMO) are of special importance since these represent the ground state and the first excited state of a molecule.

^{***} Spin quantum number (S), describes the angular momentum of the electron, that is, the direction in which the electron spins around an axis, it takes the values of $\pm 1/2$.

2.3 Light-matter interactions: *photophysics*

The physical properties of photons, the elementary particles or *quanta* of electromagnetic radiation are related to the frequency of the electromagnetic wave. The energy of a photon is dependent on its frequency as follows:

$$E = hv = \frac{hc}{\lambda} \quad (2.8)$$

Where h is the Planck constant and v is the frequency of the electromagnetic wave, which is equal to the speed of light divided by the wavelength λ .

The interaction of light with matter can be described as the interaction of the electric field component of light with the charged particles of molecules. If the magnitude of this electric field matches the energy difference between MOs, an electronic transition to a higher energy level might occur and light is said to be *absorbed*. The dipole moment operator \mathbf{R} (Eq. 2.9) of a molecule has to be considered to describe the perturbation that light creates on the electrons, because for absorption to occur the dipole moment change, represented by the transition-moment integral $R_{mn} = \langle \varphi_m | R | \varphi_n \rangle$ must not be zero.²¹

$$\mathbf{R} = e \sum_i r_i \quad (2.9)$$

A transition with $R = 0$ is said to be forbidden by selection rules which contain symmetric, spatial (overlap) and electron spin (angular momentum) requirements. For example, transitions between pure singlet and pure triplet states are strictly forbidden because the spin is not conserved. However, these forbidden transitions might become allowed by spin-orbit interactions. The probability of a transition to occur is proportional to the square of the magnitude of R_{mn} .

In quantum mechanics, the probability of a transition can be described by introducing a small time-dependent interaction (perturbation), $V(t)$, to the Hamiltonian:

$$\hat{H} = \hat{H}_0 + V(t) \quad (2.10)$$

An incident light wave interacting with an atom in an initial state φ_i could be represented by a harmonic potential $V(t) = Ve^{-i\omega t}$ which suddenly perturbs the system at time = 0. The probability for the system to lie in the final state φ_f^* , at time t , is given by the transition rate expression known as *Fermi's Golden Rule*, which is implicitly dependent on the density of the final states:

$$\lambda_{if} = \int \varphi_f^* V(t) \varphi_i \quad (2.11)$$

Using the same principles of the *Born-Oppenheimer approximation*, the energy of a molecule in each electronic states can be described as a function of the nuclear coordinates only. The graphic representation of this function is known as a potential energy surface (see figure 2.3). Here, the ground state and first excited electronic states are represented together with the overlapping vibrational states, which are the energies of the quantized periodic motions of the molecule. Because the motion of electrons and nuclei has been decoupled, electronic transitions occur vertically between points in the potential energy surfaces (*Franck-Condon principle*).²² This explains why some vibrational transitions are more intense than others depending on the overlap of the wave functions involved.

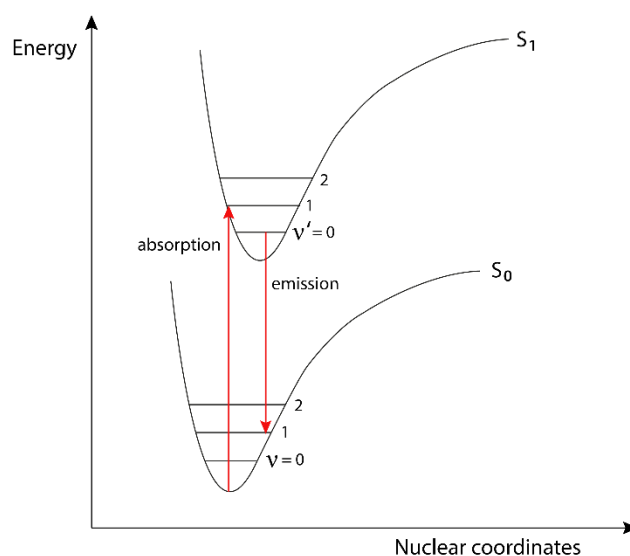


Figure 2.3 Schematic representation of the Franck-Condon principle showing potential energy surfaces of ground state and first electronic excited state.

To simply represent the different electronic states of a molecule and the transitions between them, Jablonski diagrams are often used (Figure 2.4). The main deactivation pathways of an excited state, and the corresponding reaction rate orders are shown. After absorption of a photon (10^{18} s^{-1}), rapid vibrational relaxation (10^{12} - 10^{13} s^{-1}) to the lowest vibrational level of the lowest electronically excited state will occur. As a rule, emission occurs from this lowest vibrational level because of the timescale of relaxation compared to that of emission (*Kasha's rule*). The transition between the lowest vibrational levels of the ground state is known as the 0-0 transition.

When radiation is emitted during transition between singlet states the process is called *fluorescence*, typical rate constants are in the order of 10^7 - 10^9 s^{-1} . When light is emitted during transition between states of different multiplicity the process is called *phosphorescence* and typical lifetimes are much longer, in the order of ms, because of the forbiddance of the process which is translated into slow kinetics.²³

The radiationless transition between states of the same multiplicity is known as *internal conversion* (IC) and when different multiplicities are involved the process is called intersystem crossing (ISC). Both IC and ISC are isoenergetic, meaning that the energy of the system is maintained during the transition.

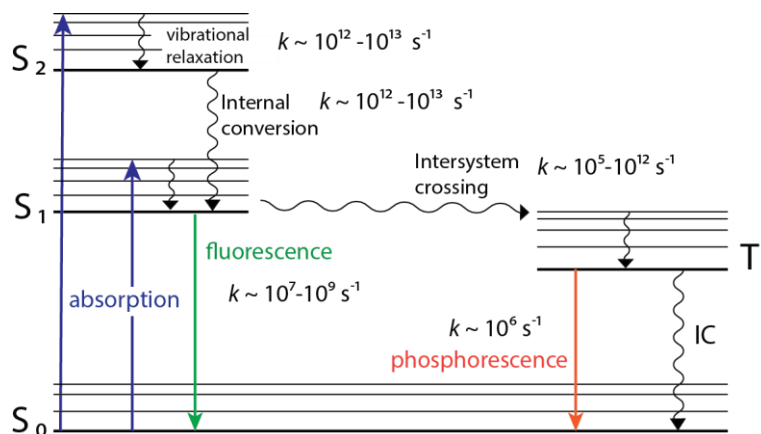


Figure 2.4 Jablonski diagram illustrating the electronic states of a molecule and the transitions between them.

The shape of absorption and emission spectra of molecules is given by the distribution of vibrational and rotational states. Because emission occurs from the lowest vibrational energy level, the maximum and absorption of emission will not appear at the same wavelength, this difference is known as *Stokes shift*. As a consequence of *Kasha's rule*, the shape of the emission spectra is typically independent of the excitation wavelength.

The kinetics of deactivation of an excited state, A^* , can be represented by the sum of the unimolecular rate constants for the deactivation process,²¹ that is:

$$\frac{-d[A^*]}{dt} = (k_r + k_{nr})[A^*] \quad (2.12)$$

where $[A^*]$ is the concentration of the excited state at time t . The mean radiative lifetime of A^* is simply the reciprocal of the sum of the rate constants:

$$\tau = \frac{1}{\sum_i k_i} \quad (2.13)$$

The efficiency of a photoinduced process is measured by its *quantum yield* (Φ), which is the number of molecules following a specific path per photons absorbed by the system. For example, the quantum yield of fluorescence is defined as the number of photons emitted divided by the number of photons absorbed, and in terms of the rate constants can be written as follows:²²

$$\Phi = \frac{k_r}{k_r + k_{nr}} \quad (2.14)$$

The process by which the quantum yield of fluorescence decreases is known as *quenching* and it can occur by different mechanisms. Collisions with the surrounding molecules, *dynamic quenching*, or the formation of non-fluorescent complexes in the ground state, *static quenching*, are two examples. The energy of the excited molecule can also be directed to alternative processes such as *electron transfer* and *energy transfer* resulting in quenching of emission.²³ Therefore, the measurement of emission properties of a chemical system is an important tool for the investigation of reactions of interest.

2.4 Excited state reactions

This work is concerned with electronic processes in the excited state of molecules. Charge separation is a primary key process in solar energy conversion, which depends on the kinetics of desired reactions such as photoinduced electron transfer, and competing processes such as energy transfer. Here, a brief description of these processes is given.

2.4.1 Energy transfer

Although energy transfer is not the focus in this thesis, it must be mentioned as a possible quenching process in which a photon is not emitted, instead, an energy exchange between a donor and an acceptor occurs, quenching the emission of the donor. Two common mechanisms of energy transfer are distinguished in the literature, *resonance energy transfer* (RET), and *Dexter energy transfer*. In the first case, a highly distance dependent dipole-dipole interaction results in energy transfer from a donor to an acceptor. Dexter energy transfer, is a short-range collisional process in which an electron is exchanged between two molecules or two parts of a molecule.

2.4.2 Photoinduced electron transfer

In photoinduced electron transfer (PET), there is an electron transfer between a donor and an acceptor where either one of them is in the excited state, resulting in a charge separated state. Because the energy of the molecule is higher in the excited state, it becomes easier for a redox reaction to occur due to a larger driving force. Intramolecular PET between a donor in the excited state and an acceptor can be represented as in equation 2.17. The direction of the electron transfer is determined by the redox potentials of the ground and excited states.²³



The Rehm-Weller equation describes the change in standard Gibbs energy for a reaction like the one presented above:

$$\Delta G = E(D/D^+) - E(A/A^-) - \Delta G_{00} - \frac{e^2}{\epsilon d} \quad (2.18)$$

where the first and second terms are the oxidation and reduction potentials of the donor and the acceptor respectively, and ΔG_{00} is the energy of the 0-0- transition of the donor. The last term is the coulombic force in the ionic pair formed after the electron transfer, where ϵ is the dielectric constant of the solvent, and d is the distance between the charges.

PET is classically described by *Marcus theory* by representing the potential energy surfaces of donor-acceptor complex and the charge-separated state as parabolic functions.²⁴ According to this theory, the excited donor-acceptor complex ($D^* | A$) moves to the charge separated state through a transition state, localized at the cross point of the potential surfaces, if the needed activation energy (ΔG^\ddagger) is supplied. Once the CS state is formed, the surrounding molecules need to reorganize until they reach a new equilibrium state dissipating some energy known as the reorganization energy λ . This energy contains contributions from nuclear configuration distortions (inner λ) and from polarization reorientation of the surrounding solvent molecules (outer λ).

The rate constant for the electron transfer can be described in terms of the electronic coupling between donor and acceptor, V_{DA} , the driving force, ΔG^0 , and the reorganization energy as follows :

$$k_{ET} = \left(\frac{\pi}{\hbar^2 k_B T} \right)^{1/2} |V_{DA}| \exp - \left[\frac{(\lambda + \Delta G^0)^2}{4\lambda k_B T} \right] \quad (2.19)$$

According to this equation, three possible cases in the Marcus model are possible²⁵: (see Figure 2.6)

- The normal Marcus region where $\lambda > \Delta G_0$, where the rate of ET increases with the driving force
- Where there is no activation barrier for the reaction, that is $\lambda = \Delta G_0$
- The inverted Marcus region where $\lambda < \Delta G_0$, the rate of the ET decreases with driving force.

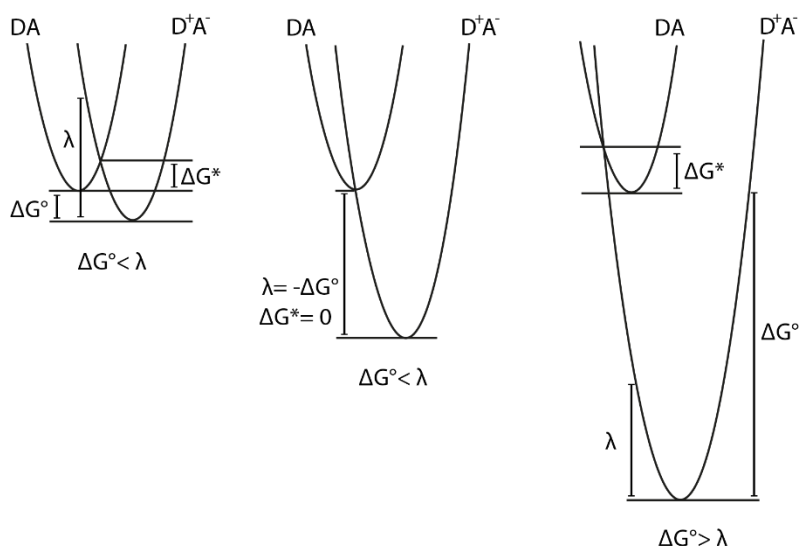


Figure 2.6 Schematic representation of Marcus theory in the normal region (left), activationless case (center) and inverted region (right). Adapted from reference 27 with permission from the publisher.

Additionally, the distinction between diabatic and adiabatic reactions is made, where the electronic coupling is large and weak respectively and thus, the probability of crossing from the lower surface on the reactants side to the lower surface on the products is either large or small.²⁶ When ET does not occur by crossing the energy barrier, it is said to occur by tunneling, and then quantum effects need to be introduced in the theory. This is known as semi-classical Marcus theory, where the rate of electron transfer is given by the density of acceptor states and the electronic coupling.

2.4.3 Interfacial electron transfer: *Semiconductor-dye interactions.*

Charge separation can be achieved by photoinduced electron transfer between molecules and metal oxide materials such as nanocrystalline TiO₂. In order to understand this process, the electronic properties of both molecules and semiconductors must be described. For molecules, the electrons are distributed in energy levels as described in section 2.2, whereas for semiconductors, the electrons are said to be distributed in *bands*. Electronic bands are combinations of the individual orbitals of the atoms forming the solid structure. Discrete energy states laying very close to each other form continuous bands. The highest occupied band form the valence band (VB), and the lowest unoccupied band form the conduction band (CB).²⁷

The band-gap is the energy by which the valence and conduction bands are separated. Contrarily to electrical conductors, where the band-gap is very small or negligible, in semiconductors the band-gap has values between 1-4 eV. Titanium dioxide (TiO₂), the most widely used semiconductor in dye-sensitized photoelectrochemical applications, has a band-gap of 3.2 eV which is considered large, and because of this it only absorbs light in the ultraviolet (UV) region.²⁸ When TiO₂ is irradiated with UV-light, electrons in the VB are photoexcited into the CB and can freely move giving the material conductive properties.

Population of the CB can also be achieved by PET from a chemically bound dye on the semiconductor, this process is known as electron injection. For this reaction to be spontaneous ($\Delta G < 0$) the energy of the excited dye should be located at more negative potentials than the CB of the semiconductor, in other words, there will be a driving force for the electron transfer to occur (see Figure 2.7).

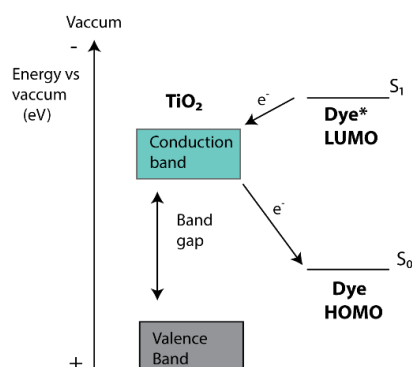


Figure 2.7 Schematic representation of energy levels of dye and semiconductor and forward and back electron transfer reactions.

For efficient charge separation in dye-sensitized semiconductors, electron injection must be fast enough to compete with the excited state decay to the ground state. This is the case for many dyes where the electron injection is ultrafast (in the order of femtoseconds) and with a quantum yield near to one. However, electron injection rates as slow as hundreds of picoseconds have been measured.²⁹ The kinetics of electron injection depends, to a great extent, on the structure of the dye; a good electronic coupling between the orbitals of the electronically excited dye and the 3d wave function manifold of the TiO₂ structure is required for ultrafast electron injection.³⁰ On the basis of Marcus theory, electron injection can be explained as the acceptor level being a continuum of available states. The charge separated state parabola then becomes a manifold of parabolas making each point of the reactant surface energy curve a transition state (see Fig 2.8). Consequently the rate ET is exclusively determined by the electronic coupling.³¹

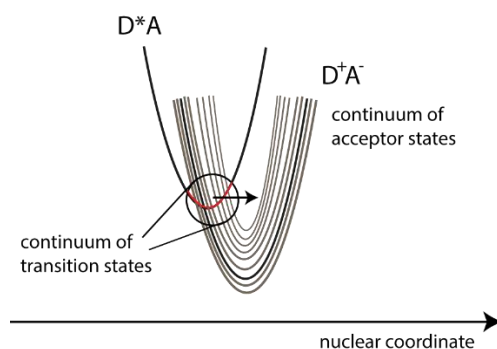


Figure 2.8 Interfacial electron transfer from a dye to the conduction band of a semiconductor explained by Marcus theory.

Back-electron transfer is the opposite of electron injection, where an electron is instead transferred from the CB of the semiconductor to the oxidized dye. As shown in Figure 2.7, the driving force this process is much larger than that of electron injection. Kinetics of back-electron transfer are typically in the order of microseconds, something that can be understood from Marcus inverted region.³⁰ Because of this, the kinetically governed charge separation in photosensitized semiconductor devices is successful, however, back-electron transfer is never avoided completely and it is an efficiency limiting process.

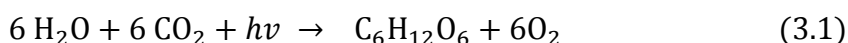
3. Approaches to solar energy conversion for fuel production

This chapter will briefly give an overview of the different approaches to solar energy conversion and storage in the form of chemical bonds.

3.1 Molecular approaches

The imitation of structure and/or functions in natural photosynthesis for the capture and storage of solar energy in the form of chemical bonds is a presumable strategy to produce renewable fuel from sun and water; this process is known as artificial photosynthesis.¹¹ Because of the complexity of the systems, research in this field is very broad and multidisciplinary. Typically, the functions of individual components are analyzed and optimized separately before their integration into multi-component molecular systems.⁸ An example of this is presented in this thesis; a molecule is designed to mimic one of the functions in natural photosynthesis; the light-driven splitting of water for the production of fuel.

In natural photosynthesis (Eq. 3.1) the energy from the sun is harvested in the center of chlorophyll molecules and transferred to a distant acceptor in the form of electrons. The electrons are given back to the chlorophyll molecules thanks to the oxygen-evolving complex (OEC) which catalyzes water oxidation into protons (H^+), electrons (e^-) and molecular oxygen (O_2). The OEC consists of a Mn_4O_5Ca complex surrounded by a protein environment that controls the parameters of the reaction and prevents the complex from degradation.³² The structure and functions of the OEC are simply fascinating because it is a key component in the natural process of solar energy conversion into fuel for life.



Creating an artificial molecular assembly able to mimic the functions of the OEC requires various essential components; an entity for the efficient capture of photons with longed-lived excited states and performing efficient charge-separation (photosensitizer),³³ an entity capable of catalyzing water oxidation^{34,35} and a smart integration of the two components to achieve efficient electron transfer and minimizing competing process, e.g. energy transfer. The basic functions of components in artificial splitting of water are illustrated in figure 3.1. The system consists of a photoactive unit (P), which transfers electrons to an acceptor unit (A). The oxidized photosensitizer gets its electron back from a donor (D), which in turn, gets electrons resulting from the oxidation of water into protons and oxygen. The components can either be separated entities or assembled into one macromolecule.

Making an efficient water splitting system is limited by significant difficulties such as instability of the molecular assemblies and the very challenging coupling of single photon absorption events to multiple redox equivalents accumulation at a molecular site.³⁶

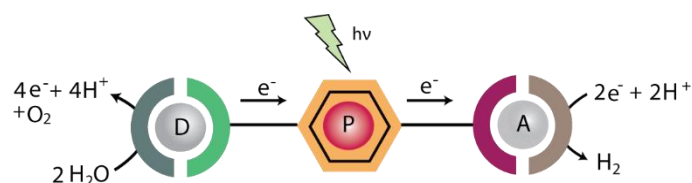


Figure 3.1 a typical scheme for artificial photosynthesis to produce hydrogen from water

3.2 Inorganic materials approaches

Conversion of solar energy to electricity was first possible by the use of semiconductor p-n junctions.[§] The most commonly used material for inorganic solar cells is silicon, but other inorganic materials such as cadmium telluride and copper indium gallium selenide are used for commercial solar cells.³⁷ The behavior of semiconductors under illumination and their use in photoelectrochemical applications is well described by using the concept of space charge region also called depletion layer.³⁸ Figure 3.2-a shows a schematic representation of a semiconductor p-n junction. When a n-doped and a p-doped semiconductor are brought into contact, a space charge region is formed at the interface, as electrons flow into the p-doped region and holes flow into the n-doped region to establish an equilibrium. Similarly, when a semiconductor is placed in contact with an electrolyte, charge carriers flow across the junction to reach equilibrium, where the chemical potential of electrons in the solid (Fermi energy, E_F) is equal to the redox potential of the electrolyte (E_{redox})²⁸, see Figure 3.2-b. In this example, electrons have moved from the bulk of the solid into the electrolyte, leaving a positive excess charge behind which produces an electric field.

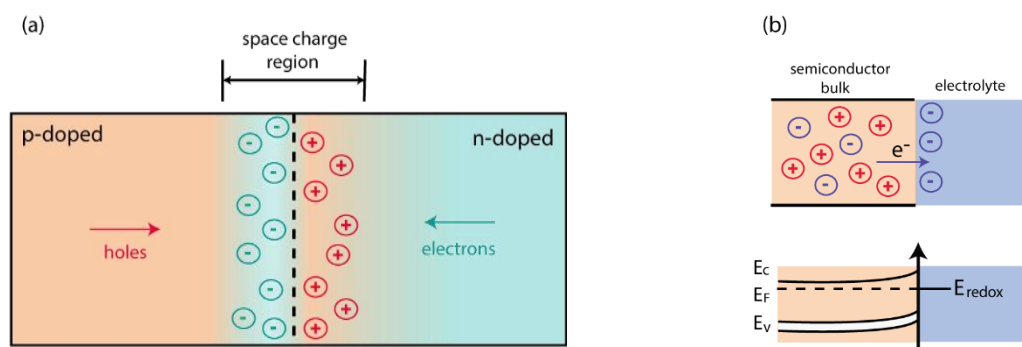


Figure 3.2 a) semiconductor p-n junction showing the space charge region. b) Electronic energy levels at the interface between an n-type semiconductor and an electrolyte containing a redox couple, showing a depletion layer resulting from electrons moving into the electrolyte. Figure adapted from reference 30 with permission from the publisher.

Under illumination, should the incident light match the band-gap of the semiconductor, electron-hole pairs will be created. Charge separation will occur due to the existing electric field

[§] An interface between an n-type and a p-type semiconductor created by introducing impurities in their structures to modify their electrical properties.

across the junction. In photovoltaics, the separated charges are extracted to an external circuit to generate work. The same principles can be applied to generation solar fuels by simply utilizing the created electrical potential difference to drive chemical reactions at a semiconductor-liquid interface.^{28,39} This is known as photoelectrochemical or photosynthetic cell. The first example of this was published by Fukushima and Honda in 1972.⁴⁰ Here, TiO_2 was used as photoanode for water oxidation and platinum was used as cathode for the reduction of protons into hydrogen, see Figure 3.3-a.

An alternative solid-material approach is to integrate the metal catalyst (co-catalyst) and the photocatalyst forming a metal-semiconductor composite.⁴¹⁻⁴³ In this case electrons are directly transferred to the catalyst and both oxidation and reduction occurs at the same site (see Figure 3.3-b). Although this approach is successful for the production of solar fuels, unfortunately, only a small portion of the solar radiation can be harvested by this method due to the large band-gap of TiO_2 and similar materials.

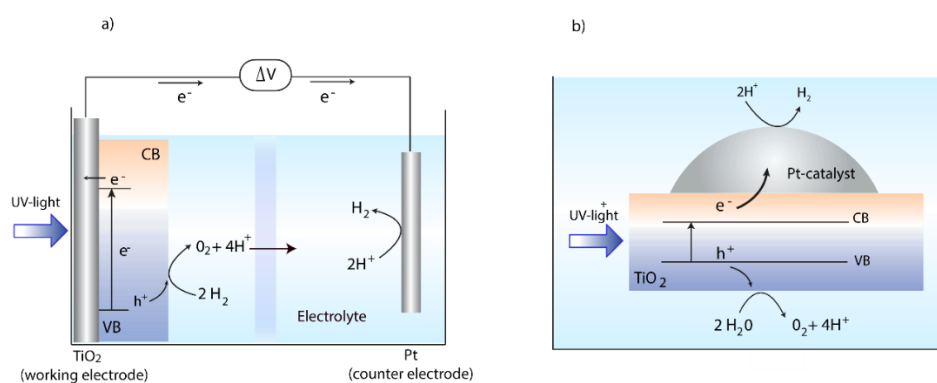


Figure 3.3 Solid-state material approaches for solar fuel production. a) Photoelectrochemical cell. b) metal-semiconductor composite

3.3 Hybrid molecular-inorganic materials assemblies

Hybrid organic-inorganic assemblies are promising tools to overcome several problems arising in both molecular and solid-state approaches. Because of the large band-gap of some semiconductors such as TiO_2 , their use is limited to the harvesting of UV light. Dye-sensitization of semiconductors makes it possible to also harvest visible light with them.⁴⁴ Further enhancement of light-harvesting in dye-sensitized semiconductors can be achieved by the use of plasmonic nanoparticles for example.⁴⁵

Efficient charge separation and accumulation of multiple redox equivalents can be achieved in dye-sensitized semiconductors by conduction band mediation.⁴⁶ Selectivity for photocatalytic reactions can be achieved by integrating molecules and solid inorganic materials into functional devices where compartmentalization of the components facilitates product obtainment and separation.^{47,48}

Two main hybrid approaches can be distinguished in the literature. The first one is a photoelectrochemical cell, such as the one shown in Figure 3.3a, where the photoanode is instead a dye-sensitized semiconductor material;⁴⁹ the cathode can either be an inorganic catalyst or a hybrid material similar to the photoanode. The second approach, is intended to achieve accumulative charge separation and conduction band mediated (CBM) electron transfer across nanocrystalline semiconductor surfaces. Here, the conduction band serves as a redox pool for the coupling of the oxidative and reductive half-reactions.⁴⁷ Figure 3.4 shows a schematic representation of conduction band mediation where the aim is to transfer the photogenerated charge to a catalyst for CO₂ reduction that is only active at highly reduced states. Although there are several reports demonstrating conduction band mediation,⁵⁰⁻⁵² to the best of my knowledge, the initiation of this process with visible light has not yet been achieved.

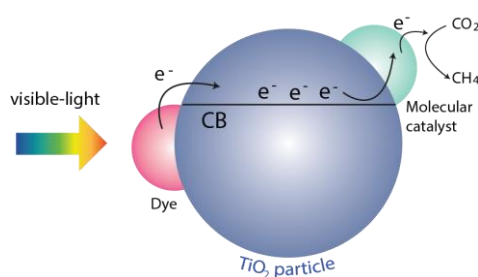


Figure 3.4 Conduction band mediated electron transfer, from dye to catalyst.

Charge separation in hybrid systems is governed by the kinetics of the interfacial dye/semiconductor/electrolyte electron transfer processes. Therefore, it is of great importance to develop strategies to control them, and especially, the competing reactions limiting the efficiency of solar energy conversion, such as back-electron transfer.

4. Experimental techniques

4.1 Electrochemical methods

4.1.1 Cyclic voltammetry

Cyclic voltammetry (CV) is a potential sweep technique for measuring the formal redox potential, $E^{0'}$, of a half reaction, which represents the potential differences between an electrode and the solution. Typically a three electrode setup is used: a reference electrode (RE) where the potential is kept constant during the measurement and is used for calibration, a working electrode (WE) where the redox process takes place, and a counter or auxiliary electrode (CE). The electrodes are immersed in a supporting electrolyte with high ionic conductivity. During a CV experiment, the potential of the WE is varied and current flows between the WE and the CE but not between the RE and the WE.⁵³ Figure 4.1 shows the variation of the potential with time in a CV program and the resulting current-potential curve for a reversible redox reaction.

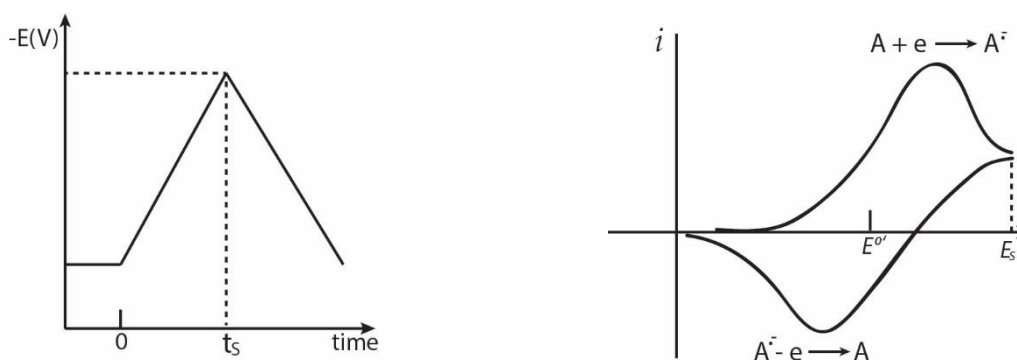


Figure 4.1 Cyclic potential sweep (left) and resulting cyclic voltammogram (right).

By subtracting the half-wave potentials of oxidation and reduction, the redox potential of chemical species can be determined. By comparing the standard redox potentials of two species, the driving force for a redox reaction can be determined. By convention, a positive potential means the reaction is spontaneous.

4.1.2 Differential pulse voltammetry (DPV)

DPV is a high sensitivity potential pulse technique based on the application of subsequent double potential pulses superimposed on a slowly changing base potential⁵⁴ as shown in figure 4.2. Contrarily to CV where current is continuously measured as the potential is swept, in DPV

current is measured twice for each point; just before the pulse and at the end of the pulse. The values of the current at these points are subtracted and plotted against the base potential. DPV is especially useful to analyze small amounts of a substance and to characterize potential peaks whose separation is very small.

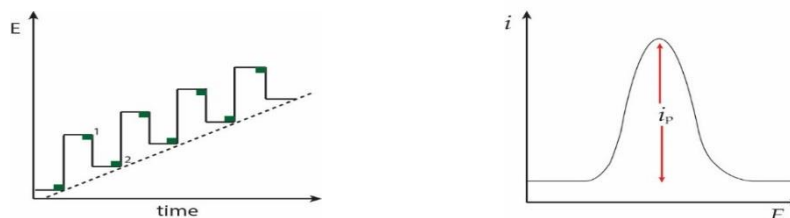


Figure 4.2 Potential excitation signal (left) and voltammogram (right) for differential pulse voltammetry.

4.1.3 Bulk electrolysis methods

A three-electrode system can also be used to constantly oxidize or reduce a chemical species. This methods have many uses in analytical and synthetic chemistry. In this work, bulk electrolysis was used to investigate the spectroscopic properties of an oxidized dye. By setting the potential at the oxidation potential of the dye, and maintaining it for a certain period of time, complete oxidation of the dye can be achieved. The spectroscopic features can be inspected during the measurement by spectroelectrochemical techniques, see section 4.3.5.

4.2 Optical spectroscopy methods

4.2.1 Steady state absorption spectroscopy

Also known as UV-vis spectroscopy, this technique consists on making a beam of continuous light pass through a sample and measuring the amount of absorbed or transmitted light at each wavelength (see Figure 4.3). According to Lambert-Beer law the absorbance, A , has a linear dependence with the product of the molar absorptivity, ϵ , the path length of the travelling light, l , and the concentration of the molecules in the solution, C , as follows:

$$A = -\log \frac{I_0}{I} = \epsilon l C \quad (3.6)$$

This linear dependency holds at relatively low concentrations ($>0.01\text{M}$) and when other optical phenomena such as scattering, emission or changes in refractive index are not interfering.

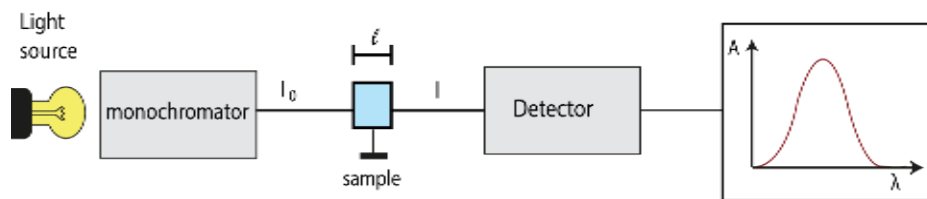


Figure 4.3 Schematic of a single beam spectrophotometer

This technique is a very versatile tool. In this work, absorption spectroscopy was used to determine the wavelength of excitation for a sample in emission spectroscopy and transient absorption spectroscopy. It was also used to control the concentration of solutions, and the amount of adsorbed dyes into highly transparent TiO₂ films. Finally, it was used to characterize oxidation reactions as described in section 4.3.5.

4.2.2 Nanosecond-transient absorption spectroscopy

Also known as flash photolysis or flash spectroscopy, this technique consist on the measurement of the absorbance of a sample, as a function of time, after excitation with a nanosecond light pulse. The difference between the absorption of the excited and ground states of the molecule is used to determine the differential absorption (ΔA).

The measurement works as follows: a short pulse of light interacts with a sample that is in the optical path of a continuous (or sometimes pulsed) source of light. The absorption of the sample is measured at short time intervals after the excitation pulse by a charge coupled device (CCD) camera. This generates charge from the incoming photons, which then is turned into a digital signal. Negative transient absorption signals appear due to ground state depopulation, and positive signals due to absorption in the excited state, see Figure 4.4a. By using a photomultiplier tube instead of a CCD, the decay of a transient signal at a specific wavelength can be measured, see Figure 4.4b. Kinetics of photoinduced reactions can be studied by this method. Figure 4.5 illustrates the nanosecond transient absorption setup used for the measurements presented in this thesis.

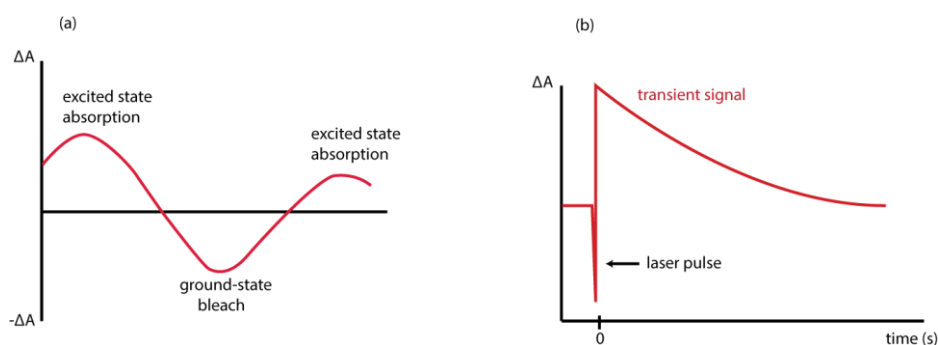


Figure 4.4. Illustration of a differential absorption spectrum (a) and a decay of a transient absorption signal (b).

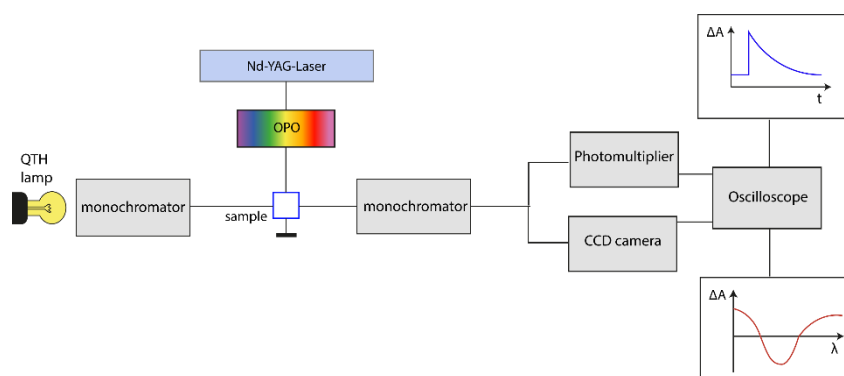


Figure 4.5 Transient absorption spectroscopy set-up for measurement of transient absorption decay.

4.3.3 Steady-state emission spectroscopy

Emission from a sample can be measured with a spectrofluorometer; a typical setup is shown in figure 4.6. The sample is excited with a continuous intense source of light, e.g. a Xe-arc lamp. The desired excitation wavelength is selected by a monochromator and specific polarization can be optionally selected before the light is directed to the sample. A beam splitter before the sample directs a part of the radiation to a reference detector in order to monitor the excitation light intensity during the measurement. This will be used to correct for fluctuations in the light source. On the detection side, the emitted photons are passed through another monochromator and collected by a photomultiplier tube. Data of emission spectra consist of an emitted photon counts as a function of wavelength. The same setup can be used to measure a so-called excitation spectra, where the intensity of emission at a single wavelength is plotted against the excitation wavelength. This is useful to investigate impurities in a sample, or the origin of unexpected emission spectra for example.

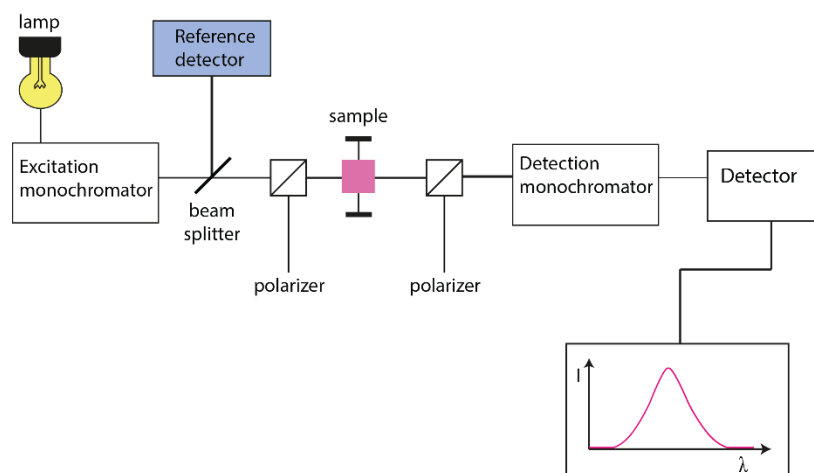


Figure 4.6 Schematic representation of right-angle spectrofluorometer setup.

4.3.4 Time correlated single photon counting (TCSPC)

Time resolved emission spectroscopy refers to the techniques used to measure the dependence of emission intensity with time. Time correlated single photon counting (TCSPC) is one of the most used techniques to measure emission decays. Figure 4.7 depicts the experimental setup for TCSPC used in this work. The sample is excited with a monochromatic pulsed diode-laser. The frequency of excitation is given by either an internal trigger in the diode driver or an external delay generator, if the emission lifetimes are too long to be measured with the default frequencies. The time that takes for emitted photons to reach the detector is measured as follows: a time to amplitude converter (TAC) generates a voltage ramp starting at time of the excitation pulse. The ramp builds up linearly with time until the arrival of an emitted photon to the detector. The voltage is amplified and converted to a numerical value by an analog-to-digital converter (ADC). The measured values are collected in a multiple-channel analyzer (MCA). The measurement is finished after collecting a desired number of events and the values are used to build a histogram of number of counts versus time.

Another data set is always recorded when performing a measurement, the Instrument Response Function (IRF). This is defined as the response of the instrument to a sample with zero lifetime⁸ and it is related to the time precision of the instrument. The resulting histogram corresponds to the shape of the excitation pulse seen by the detector. For data analysis, the IRF is deconvoluted from the intensity decay to obtain the real emission decay of the sample.

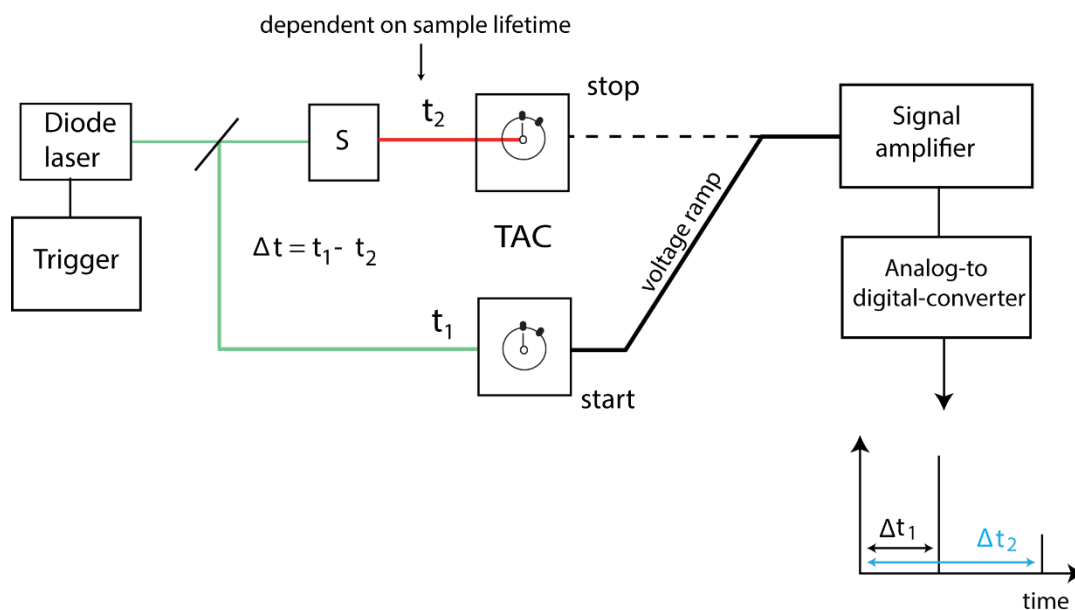


Figure 4.7 Schematic representation of time correlated single photon counting instrumentation.

4.3.5 Spectroelectrochemistry

Spectroelectrochemical techniques refer to combined experimental methods in which spectroscopic and electrochemical instruments are simultaneously used to measure an optical response induced by an applied electric field to the system. For example, in the second work presented in this thesis, bulk electrolysis was used in combination with steady state absorption spectroscopy in order to investigate the spectroscopic properties of an oxidized molecule. In this experiment the potential was fixed to the oxidation potential of the dye and the absorption changes were constantly monitored. Figure 4.8 illustrates the spectroelectrochemical setup used in this work.

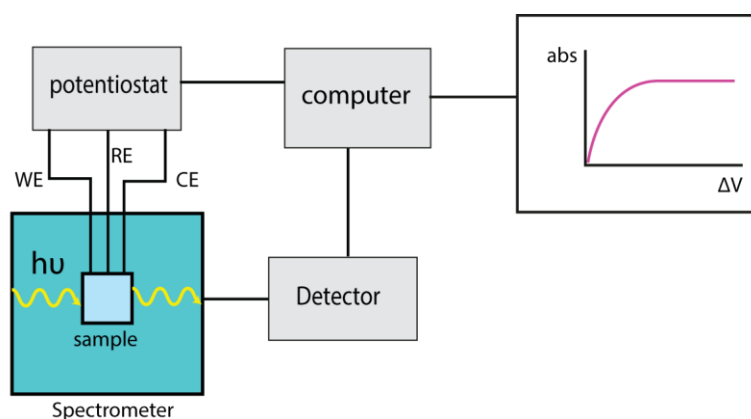


Figure 4.8 Schematic representation of a spectroelectrochemical experiment. WE: working electrode, RE: reference electrode, CE: counter electrode, abs: absorbance.

5. Results and discussion

This chapter gives a description of the research work presented in the publication and manuscript at the end of this thesis.

5.1 Molecular approach to photocatalytic water oxidation: a *Ru-Mn₂* model complex

As described in section 3.1, molecular assemblies mimicking the functions of the OEC need efficient photosensitizers and a component capable of catalyzing the four-electron oxidation of water. For a long time, tris-bpy ruthenium $[\text{Ru}(\text{bpy})_3]^{2+}$ complexes have been studied as photosensitizers and model complexes for their interesting photophysical properties. They have high extinction coefficients, long excited state lifetimes and high quantum yields of emission.³⁴ The octahedral geometry of these complexes gives interesting properties to their electronic structure, the d-orbitals in ruthenium are no longer degenerate, instead, they split into a set of two, named t_{2g} and e_g . Upon photoexcitation, these complexes undergo different electronic transitions depending on the energy of the incident light and the redox potentials of the ligands and metal, see Figure 5.1. The long excited state in these model complexes is a result of fast intersystem crossing from the singlet $^1\text{MLCT}$ state to a triplet $^3\text{MLCT}$ state. The long lifetime of the excited state, makes possible for photochemical reactions of interest, such as bimolecular charge-separation, to occur.

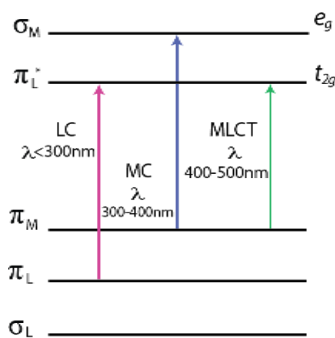


Figure 5.1 Electronic transitions in tris-bpy ruthenium complexes

For water oxidation catalysis, different types of organometallic compounds have been studied. One of them is manganese containing complexes. In a work previous to the publication presented here⁵⁵, an innovative bioinspired Mn_2 -complex was shown to be the first complex of its type, able of catalyzing water oxidation to oxygen, together with the $[\text{Ru}(\text{bpy})_3]^{3+}$ single-electron oxidant. More importantly, the complex is also able to catalyze the photochemical oxidation of water with a $[\text{Ru}(\text{bpy})_3]^{2+}$ -type photosensitizer and an external electron acceptor ($\text{Na}_2\text{S}_2\text{O}_8$), see Figure 5.2.

5.1.2 Electrochemical characterization

The electrochemical properties of compounds were studied by means of DPV in phosphate buffer (pH 7.2). Signals attributed to ligand-based and metal-based oxidation of the ruthenium centre were observed for the ligand complexes and the dyad, see table 5.1.

Table 5.1 Electrochemical data for 7 a-c and 8c.

Compound	Ligand-based oxidation E (V vs. NHE)	Metal-based oxidation E (V vs. NHE)
7a	0.86	1.38
7b	0.87	1.60
7c	0.97	1.56
8c	0.80	1.6

As expected, the introduction of the electron-withdrawing imidazole-phenanthroline-type ligand resulted in higher metal-centered oxidation potentials in 7a-c compared to parent compounds based on $[\text{Ru}(\text{bpy})_3]^{2+}$ (1.26 V vs NHE). Also, for the ligand complexes containing electron-withdrawing ester groups on the bpy ligands, the oxidation potentials are shifted toward positive values. Such observation has been already reported with other $[\text{Ru}(\text{bpy})_3]^{2+}$ -type complexes (for details see Paper I). For the dyad, apart from the two oxidation signals, a catalytic current was observed at about 1.2 V vs NHE suggesting activity for water oxidation. However, upon irradiation with visible light, in the presence of an external acceptor (sodium persulfate), no catalytic current was observed.

5.1.3 Photophysical characterization: absorption and emission properties

For the photochemical water oxidation to work, photoinduced electron transfer to an external acceptor from the ruthenium photosensitizer, and subsequent regeneration of the oxidized chromophore, by electron-transfer from the attached manganese complex is needed. By studying the photophysical properties of the complexes, we could understand the origin of the photochemical water oxidation failure.

Figures 5.4-5.5 show the absorption spectra of the ligand complexes 7a-c and the Ru-Mn₂ dyad 8c. The π - π^* transitions in the bpy ligands are observed as an intense band at around 300 nm. Mainly the metal-to-ligand charge transfer absorption band, located at around 400 nm was affected by pH, which was a first indication that the electronic states of the complex ligands were strongly pH dependent.

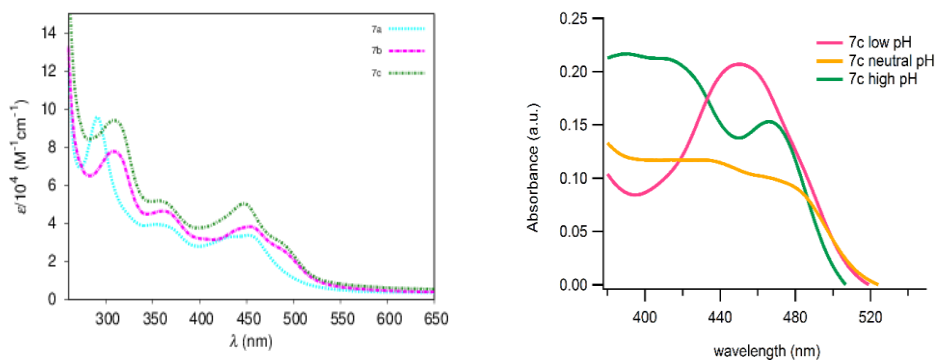


Figure 5.4 Absorption spectra of the ligand complexes 7a-c in a mixture of acetonitrile/water (1:1 v/v) (left), and complex 7c in the same mixture at different pH values.

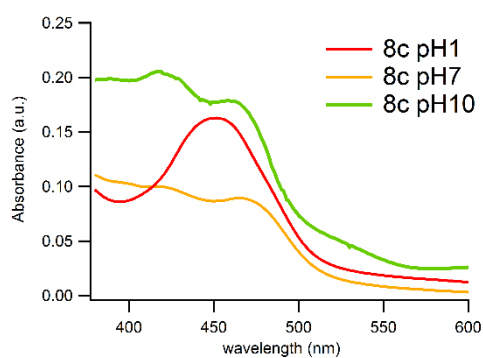


Figure 5.5 Absorption spectra of the Ru-Mn₂ dyad 8c in a mixture of acetonitrile/water (1:1 v/v) at different pH values.

As mentioned before, the ligand-complexes showed very short lived excited states, including complex 7c, which was designed to decrease the planarity and the conjugation in the system, see Figure 5.6

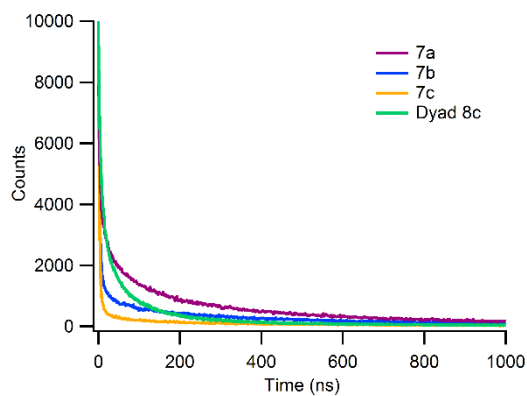


Figure 5.6 Time-resolved emission decay traces for 7a-c and the dyad 8c in a deaerated 1:1 mixture of acetonitrile/water (v/v).

All compounds displayed a characteristic triplet metal-to-ligand charge transfer ($^3\text{MLCT}$ emission). The emission properties of all the compounds were also affected by pH (see Figure 5.7). Interestingly, 7c clearly showed two emission peaks at neutral conditions. This peak was removed at acid conditions and increased at high pH. The corresponding dyad also showed two emission peaks at high pH conditions. The dual emission observed in these complexes could be explained by the pH-dependent structural characteristics arising from the introduction of the phenol. Different isomers, depending on the protonation states could exist in equilibrium. This model is supported both by literature findings^{59,60} and our DFT calculations.

It is important to mention that the peak centered around 450 nm in 7c was also removed upon addition of $\text{Mn}(\text{OAc})_2$ which is an indication of formation of the dyad 8c, where that peak is not present in neutral conditions. This corroborates the presence of manganese in dyad 8c.

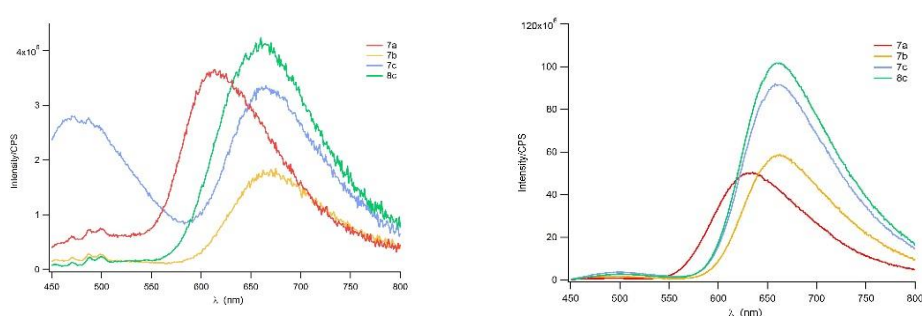


Figure 5.7 Emission spectra of 7a-c and the dyad 8c at neutral conditions (top left) and pH=1 (top right) and pH=10 (bottom).

Excitation spectra of 7c at the wavelengths of the two different emission peaks suggested that there are two emissive species with different ground-state precursors (see Figure 5.8).

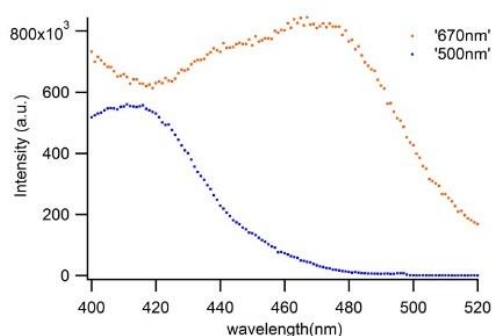


Figure 5.8 Excitation spectra of 7c in a deaerated 1:1 mixture of acetonitrile/water (v/v) at two different emission maximum

The ligand complexes and dyad containing electron withdrawing $(\text{COEt})_2\text{bpy}$ ligands (7b-c and 8c), have red-shifted emission maximum in neutral conditions compared to that of the ligand complex 7a. Also, contrarily to complex 7a, the emission maxima for 7b-c and 8c, were not significantly affected by pH. This supports the statement that the excited state is localized at

the (COEt)₂bpy ligands for the complexes that contain them; since pH changes mainly affect the hydroxyl and carboxylate groups localized far away from the ruthenium moiety. It also indicates that the excited state of 7a more likely resides there, at the phenantroline-bansimidazole part.

Time-resolved emission spectra of the complexes showed complex decay patterns which are strongly dependent on pH and all the compounds were strongly quenched (Figure 5.9), including their precursors (5a-c). The quenching was more significant at high pH for the 7-series.

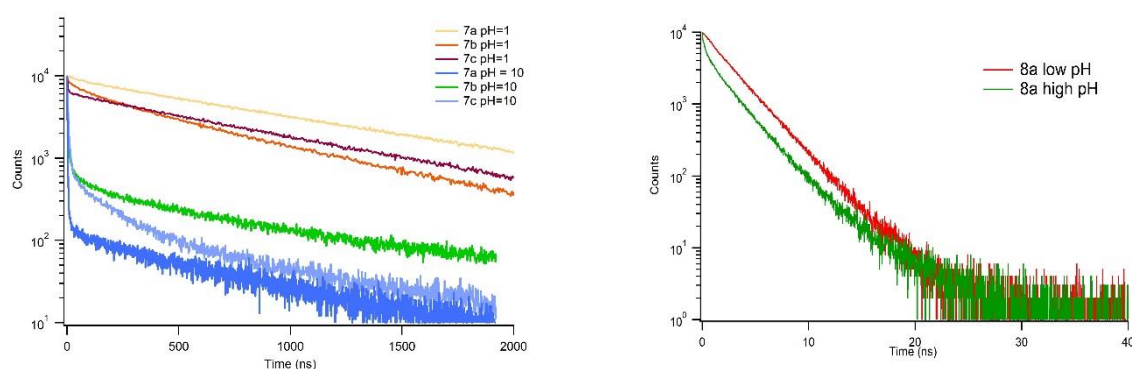


Figure 5.9 Time-resolved emission decay traces for 7a-c and the dyad 8c in a deaerated 1:1 mixture of acetonitrile/water (v/v) at different pH conditions.

5.1.4 Undesired excited state reactions explain the unsuccessful water oxidation.

The excited-state properties of the compounds are responsible for the observed photochemical behavior, and therefore a detailed analysis of the processes that take place in the excited state is needed. The short excited-state lifetimes of the ligand-complexes and the Ru-Mn₂ must be a result of a quenching process. For the dyad, this could be explained by efficient quenching from the manganese, because the ruthenium and manganese centres are in very close proximity. However, from our measurements, it was clear that the quenching was also very efficient in the absence of manganese, and that the photophysical behaviour for all compounds was complex, including the precursors (5a-c) and therefore it was evident that the expected emission properties of the (Ru[bpy]₃)²⁺-type ligands were already affected by the introduction of the phenol moiety, and this would be corroborated with the strong pH-dependence of the emission properties. Take the example of compound 5a, where bi-exponential decay at neutral conditions was observed. At low pH, the emission quantum yield increased and the long-lived components of the decay that could be attributed to unperturbed ³MLCT emissions were favored. By contrast, the short-lived components are favored at high pH. This trends were observed for all the studied compounds.

Density functional theory (DFT) theoretical calculations for compounds 5a and 7a suggested that a strong hydrogen bonding and even an intramolecular proton transfer from the phenol to the imidazole group is likely to occur. This would result in formation of a phenolate, which plays an important role in explaining the pH-dependent photophysical behavior of the compounds. If the quenching is resulting from electron-transfer from this part of the molecule, the quenching must be more efficient at high pH, since more negative charges would be accumulated around the phenol group, increasing the efficiency of electron transfer to the oxidized ruthenium centre. It was therefore evident, that by linking the photosensitizer moiety to the phenol and imidazole motifs, the quenching becomes stronger.

The introduction of the phenyl ring in the ligand complex 7c and in dyad 8c, which was aiming to decrease the conjugation in the ligands to disrupt the electron transfer, did not have an appreciable effect in the photophysical behavior of the compounds. As mentioned before, the design strategy was successful in delocalizing the ³MLCT excited state around the (CO₂Et)₂bpy ligand, further away from the manganese centre. However, this was not enough to prevent the strong quenching.

The dual emission observed in some of the complexes is also in agreement with the discussion above, since at low pH, the degree of protonation comes to saturation avoiding the formation of the phenolate which could explain the absence of the dual emission. In that case, the complex behavior of the ligand-complexes (7a-c) and the precursors (5a-c) could be explained by an excited state proton transfer mechanism, and in fact, it has been previously reported that benzimidazole derivatives can undergo this process extremely fast. However, this could be only confirmed by performing ultrafast transient spectroscopy studies.

To summarize, the design of the structures was successful in creating compounds where the excited state is localized further away from the Mn-Mn moiety, however it was not successful in avoiding communication between this part of the molecule and the ruthenium center; as a result, strong electron-transfer quenching of the excited state takes place at neutral conditions, which explains why the photochemical water oxidation was not successful in dyad 8c.

5.2 Interfacial electron transfer in dye-sensitized TiO₂ nanoparticles.

In this work, photoinduced electron transfer from TiO₂ to an organic dye was studied. The effects of surrounding electrolytes were investigated to explore the possibility of controlling back-electron transfer by structural-related properties such as viscosity, polarity and steric effects. We selected room temperature ionic liquids (ILs) for this. Because of their high conductivity, negligible volatility and high thermal and electrochemical stability, they have gained attention to replace organic solvents in photovoltaic applications, especially, dye-sensitized solar cells (DSSC).^{57,58} The composition of ILs affects the interfacial electron transfer processes between the dye and the semiconductor.^{59,60} Because the performance of these devices depends on the kinetics of these interfacial processes, it is of importance to understand the role that ILs play at the dye-semiconductor interface. We have studied the back-

electron transfer because it is an efficiency-limiting process in solar energy conversion, and also because we can gain information about how the ILs interact with the surface by studying this process. Should ILs have a positive effect, they could be used to obtain longer lived charge-separated states in dye-sensitized semiconductors. This would be advantageous to solar energy conversion approaches where accumulative charge separation is needed, as previously described in section 3.3.

An example of this, is the reduction of an iron metalloporphyrin (Fe-protoporphyrin-IX) through TiO₂-conduction band mediation. By sensitizing TiO₂ with an organic dye (D35) the photoinduced electron transfer is initiated with visible-light. A schematic representation of this is shown in Figure 5.7. The aim is to control the interfacial electron transfer kinetics to store electrons in the conduction band as long as possible, so that they can be transferred further to the porphyrin. This is a work in progress, where different processes and variables are being studied. Here, we solely report a study concerning the back-electron transfer.

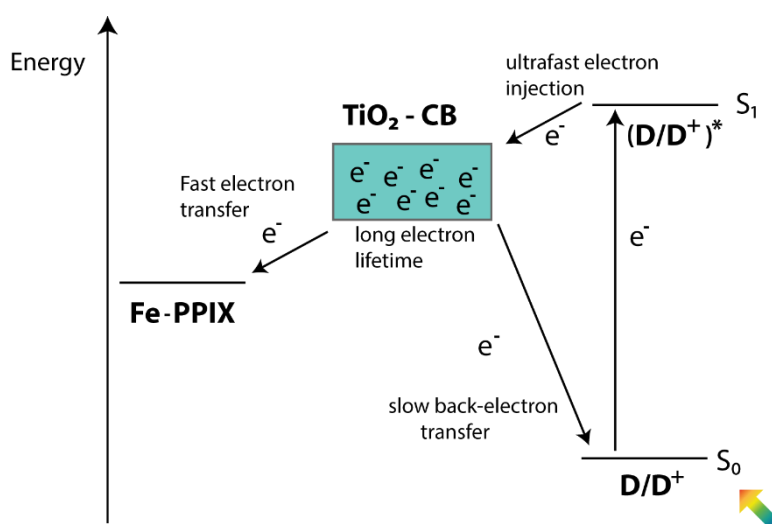


Figure 5.7 Illustration of ideal conduction band mediated electron transfer from a dye to an electron acceptor.

5.2.1 Description of the molecular-inorganic material assembly

The organic metal-free D35 dye has a donor-link-acceptor structure type, in which efficient intramolecular electron transfer occurs from the triphenylamine moiety to the cyanoacrylic acid acceptor group, which also functions as anchoring group for TiO₂,⁶¹ see Figure 5.8.

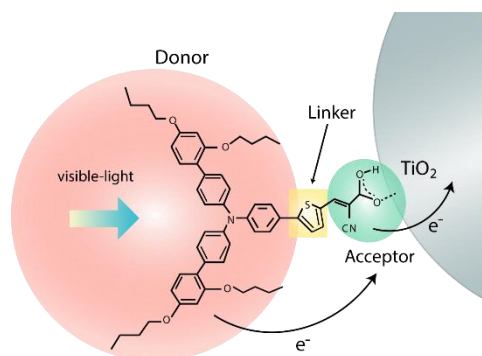


Figure 5.8 Donor-linker-acceptor structure of D35.

The dye molecules are chemically adsorbed onto mesoporous[≈] TiO₂-nanoparticulate thin films (4-7 μ m thick) by simply immersing the films in a solution of the dye. The films are typically semitransparent which allows for spectroscopic characterization. The high-porosity and large surface area of the TiO₂ material is advantageous since a great amount of dyes per nanoparticle can be adsorbed, resulting in enhanced light harvesting.

Upon dye excitation, electron injection to the conduction band of TiO₂ occurs. If the charge is not extracted to an external circuit, as in the case of DSSCs, or transferred further to an acceptor, the electrons in the CB will eventually recombine to the oxidized dye. In efficient dye-sensitized solar cells (DSSC), this process is not of much importance since the regeneration of the oxidized dye by a redox electrolyte is much faster (~100 times) than the recombination. On the other hand, if the goal is to transfer the electrons to an acceptor, which is either anchored to the TiO₂ surface or in solution, back-electron transfer becomes the main competitive route.

5.2.2 The use of ionic liquid electrolytes to control back-electron transfer kinetics

There is a number of factors that can affect the kinetics of back-electron transfer in dye-sensitized semiconductor interfaces. One of them, is the properties of the surrounding environment. It is known that the polarity of the solvent has an effect on the kinetics of recombination in DSSC.⁶² However, to the best of my knowledge, the influence of ILs on the kinetics of back-electron transfer has not been reported before.

In this study, the possibility of using room temperature ionic liquids (ILs) to control the kinetics of back-electron transfer was explored. 1-alkyl-3-methylimidazolium- based ILs were chosen. The rates of the back-electron transfer were compared to that in the presence of acetonitrile and 0.1 M LiClO₄.

[≈] That contains pores between 2-50 nm

We hypothesized that bulky cations contained in ILs can serve as a blocking layer protecting the dye from recombination as they will temporarily reorient and accumulate at the charged TiO_2 surface. A schematic representation of this is shown in figure 5.9. Compared to for example the small lithium (Li^+) ions in organic solvent electrolytes, cations in the ILs should be more prone to form layered structures at the charged interface.⁶³ If this is true, the kinetics of the back-electron transfer should be slower in the presence of these cations compared to the kinetics in the presence of Li^+ .

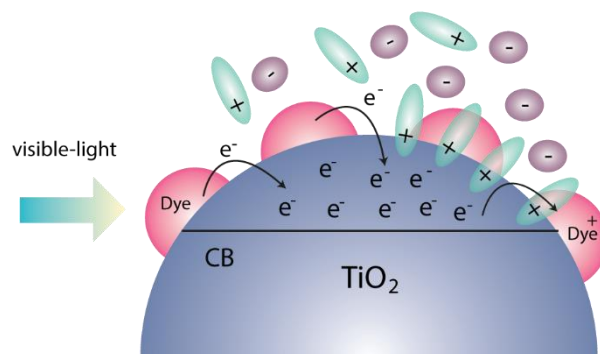


Figure 5.9 Schematic representation of back-electron transfer in D35-sensitized TiO_2 and the effect of the cations in ionic liquids.

The kinetics of back-electron transfer in D35-sensitized TiO_2 thin films, were probed with nanosecond transient absorption spectroscopy. The spectroscopic features of the ground-state bleach and oxidized dye are shown in Figure 5.10. The kinetics were probed between 600-680 nm, where the oxidized dye has the main contribution to the absorbance. The kinetics were also probed at the wavelength of the ground state bleach (540 nm), the resulting kinetics were different and somewhat more difficult to interpret, given that no specific trends were found. Possibly, a Stark-effect[‡] dominating contribution could explain this behavior,⁶⁴ however, no details will be given here since this will be a separate subject for future work. As it can be seen in Figure 5.11, the kinetics of back electron transfer are slower in the presence of 1-butyl-3-methylimidazolium hexafluorophosphate (BMIMPF_6) compared to that in acetonitrile. The kinetics are even slower in the presence of an IL containing a larger cation; 1-hexyl-3-methylimidazolium hexafluorophosphate (HMIMPF_6) (see Figure 5.12). Numerical values of the kinetic rate constants of transient absorption decays are shown in table one. The values were obtained by fitting the decays to double-exponential functions.

[‡] “The change of spectra of atoms and molecules due to the presence of an external electric field”[64].

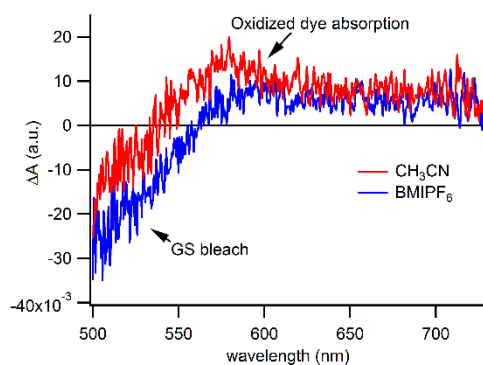


Figure 5.10 Transient absorption spectra of D35- sensitized TiO₂ probed after 100 ns of the 520 nm excitation pulse.

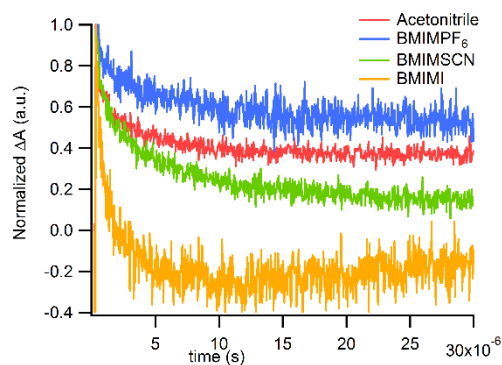


Figure 5.11. Kinetic traces of D35-sensitized TiO₂ thin-films on glass in contact with acetonitrile, BMIPF₆ and BMIMSCN, recorded at 600 nm.

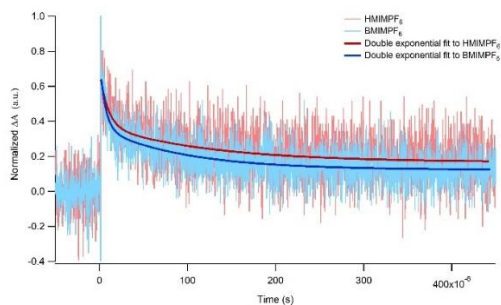


Figure 5.12. Kinetic traces for D35-sensitized TiO₂ thin-films in contact with BMIPF₆ (blue) and HMIMPF₆ (red) probed at 680 nm and corresponding double exponential fits.

Table 1. Kinetic rate constants of transient absorption decay, in D35-sensitized TiO₂, probed at 680 nm.

Sample	A1[%]	k_{obs} [10^5 s ⁻¹]	A2[%]	k'_{obs} [10^5 s ⁻¹]
HMIMPF ₆	50±5	1,7 ± 0,9	50±4	0,07 ± 0,01
BMIMPF ₆	50±9	1,5 ± 0,5	49±9	0,14 ± 0,06
CH ₃ CN	60±4	2,4 ± 0,3	40±4	0,24 ± 0,05
0.1 M LiClO ₄	53±3	5,9 ± 4,2	47 ± 3	0,41 ± 0,11

As it can be seen in table 1, the rate constants of back-electron transfer are smaller in the presence of HMIMPF₆ and BMIPF₆ compared to those in the presence of acetonitrile and LiClO₄. This seemed to be in accordance to our initial hypothesis, however, this had to be

corroborated by the exclusion of other effects such as viscosity and differences in the efficiency of electron injection. As described in the manuscript, viscosity effects were excluded by comparing to the back-electron transfer kinetics in the presence of a quasi-solid electrolyte based on polyacrylonitrile, ethyl carbonate and propyl carbonate, which has a viscosity at least three order of magnitude higher than the viscosity of the studied ionic liquids.⁶⁸ A much faster decay, compared to that in the presence of iodide was observed, and therefore, high viscosity was ruled-out as the main reason for slowed back-electron transfer. Differences in electron injection efficiency were neither responsible for the slower kinetics, as demonstrated by comparing the initial intensities of the kinetic traces. Thus, the initial hypothesis seemed to be adequate to explain the results.

The faster observed decay of the oxidized dye signals in the presence of 1-butyl-3-methylimidazolium hexafluorophosphate (BMIMSCN) and 1-butyl-3-methylimidazolium hexafluorophosphate (BMIMI) could be attributed to regeneration of the oxidized dye by the I_3^-/I^- and SCN_2/SCN^- redox couples, as it is reported in the literature and corroborated by spectroelectrochemical experiments, see Figure 5.13.^{65,66} When D35 is electrochemically oxidized, spectral signatures of the oxidized dye are observed at around 400, 600 and from 700-1000 nm. Upon addition of BMIMSCN and BMIMI these spectral features disappear and the spectroscopic signatures of the ground-state dye are observed again.

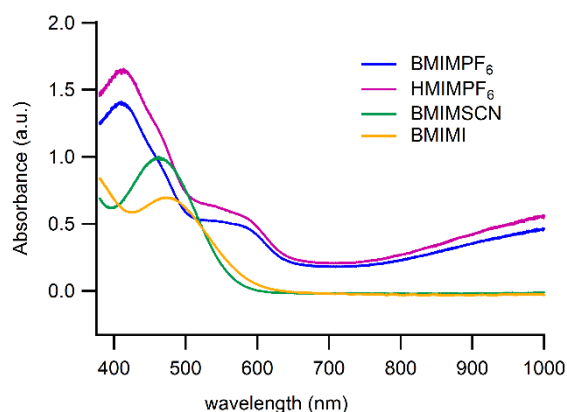


Figure 5.13 Absorption spectra of D35 on TiO₂ in the presence of the ILs after electrochemical oxidation.

To summarize, the slower kinetics of back-electron transfer in the presence of ionic liquids containing bulky, 1-alkyl-methylimidazolium cations, and inert anions has been demonstrated. We propose a mechanism where the reorganization of cations near to the charged TiO₂ surface have a temporal screening effect on the columbic attraction between the electrons in the conduction band and the oxidized dye. We suggest that this idea is interesting to be further explored as a possible strategy to obtain longer-lived charge separated states in dye-sensitized semiconductor assemblies for solar energy conversion.

6. Summary and future perspective

This work was devoted to the understanding of excited states reactions in molecular and molecular-material assemblies for solar energy conversion. Two different systems were studied. The first one, a model complex for artificial water splitting, was showed to be unsuccessful due to intramolecular, competitive electron transfer processes within the molecular assembly.

In the second work, it was shown that ionic liquids can be used to control interfacial electron transfer processes in dye-sensitized mesoporous TiO_2 , by taking advantage of the size and polarization of the ions. This idea can potentially be used to achieve longer charge separated states which are needed for multi-electron photocatalytical reactions to obtain solar fuels.

By comparison of these studies, and the analysis of the studied literature, it can be concluded that although molecular design offers control and tuning of spectroscopic and photophysical properties of photosensitizers and catalysts, in general, the electron transfer processes in purely molecular assemblies for solar energy conversion are very difficult to understand and control due to their complexity. On the other hand, electron transfer processes in hybrid molecular-semiconductor assemblies are more easily controlled and understood, due to the existence of several interfaces which can be easily modified by the introduction of additives or by slightly modifying the structure of their components. Therefore, by combining the design potential of molecules, and the beneficial charge separation properties of semiconductors, hybrid molecular-inorganic material approaches for solar energy conversion become advantageous alternatives that deserve much effort in solar fuels research.

The continuation of this project will focus in further exploration of strategies to achieve long-lived charge separated states in dye-semiconductor interfaces. Future studies will comprise: the study of cation-semiconductor interface interactions through the analysis of kinetics of back-electron transfer and the Stark effect. We will continue studying ionic liquid and gel-based electrolytes. In parallel, we will study conduction band mediation in molecular-semiconductor assemblies, where the aim is to achieve visible-light induced electron transfer from a dye to a model catalyst.

Acknowledgements

I would like to thank the following persons who have helped me and accompanied me during my PhD studies:

My supervisor, Maria Abrahamsson, for giving me the opportunity of being part of her research group, letting me contribute to the very interesting and exciting field of solar energy conversion. Thanks for all your support through hard times and for your very valuable contributions to the improvement of my writing, planning and scientific thinking skills.

Bo Albinsson, Joakim Andreasson, Per Lincoln, Maurizio Furlani and Gerrit Boschloo for the helpful and interesting scientific discussions and support.

My near colleagues Joachim, Melina, Daniele, Jens and Rita for their valuable collaboration, help and interesting discussions.

Damir Dzebo for helping me out of my “very difficult” technical/IT-related problems, and for all the laughs and funny moments to remember.

Laura de Battice for the unconditional support, friendship and all the fun!

All other colleagues and ex-colleagues at the department for being nice people!

My family in Mexico for their love and support.

And finally, my dearest of all, Mattias, for everything you have done for me.

References

- (1) Doran, P. T.; Kendall, M. *Eos* **2009**, *90*, 22.
- (2) Anderegg, W. R. L.; Prall, J. W.; Harold, J.; Schneider, S. H. *PNAS*. **2010**, *107*, 12107.
- (3) Petherick, A. *Nature Climate Change* **2013**, *3*, 436.
- (4) International Energy Agency. Key World Energy Statistics. 2014.
- (5) Timilsina, G. R.; Kurdgelashvili, L.; Narbel, P.A. *Renewable and Sustainable Energy Reviews*. **2012**, *16*, 449.
- (6) Bequerel, E. *C.R. Acad. Sci.* **1839**, *9*, 145.
- (7) Kärkäs, M. D.; Verho, O.; Johnston, E. V.; Åkermark, B. *Chem. Rev.* **2014**, *114*, 11863.
- (8) Tachibana, Y.; Vayssieres, L.; Durrant, J. R. *Nature Photonics* **2012**, *6*, 511.
- (9) Corma, A.; Garcia, H. *Journal of Catalysis*. **2013**, *308*, 168.
- (10) Morris, A. J.; Meyer, G. J.; Fujita, E. *Accounts of Chemical Research* **2009**, *42*, 1983.
- (11) Sun, L.; Hammarström, L.; Åkerman, B.; Styring, S. *Chemical Society Reviews*. **2001**, *30*, 36.
- (12) Rieger, P. H. *Electrochemistry*; 2nd ed., 1994.
- (13) Arnaut, L. F., S.; Burrows, H. *Chemical Kinetics. From Molecular Structure to Chemical Reactivity*; Elsevier, 2007.
- (14) Hood, J. *Philosophical Magazine* **1878**, *Volume 6, Series 5*, 371.
- (15) Arrhenius, S. *Zeitschrift für Physikalische Chemie* **1889**, *4*, 226.
- (16) Van't Hoff, J. *Studies in Chemical Dynamics*. Frederik Muller & Co: Amsterdam, 1896.
- (17) Atkins, P.; De Paula, J. *Physical Chemistry*. 8th ed. Oxford: UK, 2006.
- (18) Arrhenius, S. *Philosophical Magazine and Journal Science*. **1896**, *41*, 237.
- (19) Arrhenius, S. Nobel Lecture: Development of the theory of electrolytic dissociation. http://www.nobelprize.org/nobel_prizes/chemistry/laureates/1903/arrhenius-lecture.html (2015-05-15).
- (20) Leach, A. R. *Molecular modelling. Principles and applications*; 2nd ed.; Pearson Education Limited, 2001.
- (21) Turro, N. *Molecular Photochemistry*. W.A. Benjamin, Inc.: **1965**.
- (22) Hollas, M. J. *Modern Spectroscopy* 4th ed., **2004**.
- (23) Lakowicz, J. R. *Principles of fluorescence spectroscopy*; 3rd ed.; Springer Science+Business Media, **2006**.
- (24) Marcus, R. A. *Reviews of Modern Physics* **1993**, *65*, 599.
- (25) Metzger, R. M. *J. Mater. Chem* **2008**, *18*, 4364.
- (26) Barbara, P. F.; Meyer, T. J.; Ratner, M. A. *Journal of Physical Chemistry*. **1996**, *100*, 13148.
- (27) Bard, A. J. F., L.R. *Electrochemical methods*; 2nd ed., 2001.
- (28) Gratzel, M. *Nature* **2001**, *414*, 338.
- (29) Koops, S. E.; O'Regan, B. C.; Barnes, P. R.; Durrant, J. R. *J. Am. Chem. Soc.* **2009**, *131*, 4808.
- (30) Hagfeldt, A.; Grätzel, M. *Chemical Reviews*. **1995**, *95*, 49-68.
- (31) Kalyanasundaram, K. *Dye-sensitized Solar Cells*; EPFL Press, **2010**.
- (32) Najafpour, M. M.; Govindjee. *Dalton Transactions*. **2011**, *40*, 9076.

- (33) Abrahamsson, M., *Tuning of the Excited State Properties of Ruthenium (II)-Polypyridil Complexes*. Uppsala University, **2006**. ISSN: 1651-6214.
- (34) Wang, H.-Y.; Mijangos, E.; Ott, S.; Thapper, A. *Angew. Chem. Int. Edit.* **2014**, *53*, 14499.
- (35) Kärkäs, M. D.; Johnston, E. V.; Karlsson, E. A.; Lee, B. L.; Åkermark, T.; Shariatgorji, M.; Ilag, L.; Hansson, Ö.; Bäckvall, J.-E.; Åkermark, B. *Chem-Eur J.* **2011**, *17*.
- (36) Karlsson, S. *Single and Accumulative Electron Transfer - Prerequisites for Artificial Photosynthesis*. Uppsala University, 2010. ISSN: 1651-6214.
- (37) Green, M. A. *J. Mater. Sci: Mater. Electron.* **2007**, *18*, S15.
- (38) Gerischer, H. *J Electrochem. Soc.* **1966**, *113*, 1174.
- (39) Paracchino, A.; Laporte, V.; Sivula, K.; Grätzel, M.; Thimsen, E. *Nature Materials* **2011**, *10*, 456.
- (40) Fujishima, A.; Honda, K. *Nature* **1972**, *238*, 37.
- (41) Domen, K.; Kudo, A.; Shinozaki, A.; Tanaka, A.; Maruya, K.; Onishi, T. *J. Chem. Soc., Chem. Commun.* **1986**, 356.
- (42) Syama, K.; Arakawa, H. *J. Phys. Chem.* **1993**, *97*, 531.
- (43) Ran, J.; Zhang, J.; Yu, J.; Jaroniec, M.; Qiao, S. Z. *Chem. Soc. Rev.* **2014**, *43*, 7787.
- (44) O'Regan, B., Grätzel, M. *Nature* **1991**, *353*, 737.
- (45) Brown, M. D.; Suteewong, T.; Kumar, R. S. S.; D'Innocenzo, V.; Petrozza, A.; Lee, M. M.; Wiesner, U.; Snaith, H. J. *Nano letters* **2011**, *11*, 438.
- (46) Karlsson, S. *J. Am. Chem. Soc.* **2010**, *132*, 17977.
- (47) Hammarström, L. *Accounts of Chemical Research.* **2015**, *48*, 840.
- (48) Schreier, M.; Gao, P.; Mayer, M. T.; Luo, J.; Moehl, T.; Nazeeruddin, M. K.; Tilley, D. S.; Grätzel, M. *Energy & Environment Science* **2015**, *8*, 855.
- (49) Alibabaei, L.; Brennaman, M. K.; Norris, M. R.; Kalanyan, B.; Song, W. J.; Losego, M. D.; Concepcion, J. J.; Binstead, R. A.; Parsons, G. N.; Meyer, T. J. *PNAS* **2013**, *110*, 20008.
- (50) Ardo, S.; Achey, D.; Morris, A. J.; Abrahamsson, M.; Meyer, G. J. *J. Am. Chem. Soc.* **2011**, *133*, 16572.
- (51) Obare, S. O.; Ito, T.; Meyer, G. J. *J. Am. Chem. Soc.* **2006**, *128*, 712.
- (52) Staniszewski, A.; Morris, A. J.; Ito, T.; Meyer, G. J. *J Phys Chem B* **2007**, *111*, 6822.
- (53) Evans, D. H. O. C., K.M.; Peterson, R.A.; Kelly, M.J. *Journal of Chemical Education* **1983**, *60*, 290.
- (54) Molina, A.; Laborda, E.; Rogers, E.; Martínez-Ortiz, F.; Serna, C.; Limon-Petersen, J. G.; Rees, N. V.; Compton, R. G. *Journal of Electroanalytical Chemistry.* **2009**, *634*, 73.
- (55) Karlsson, E. A.; Lee, B.-L.; Åkermark, T.; Johnson, E. V.; Kärkäs, M. D.; Sun, J.; Hansson, Ö.; Bäckvall, J.-E.; Åkermark, B. *Angew. Chem. Int. Ed.* **2011**, *50*, 11715.
- (56) McClanahan, S. F.; Kincaid, J. R. *J. Am. Chem. Soc.* **1986**, *108*, 3840.
- (57) Gorlov, M., Kloo, L. *Dalton Transactions.* **2008**, 2655.
- (58) Zakeeruddin, S. M.; Gratzel, M. *Advanced Functional Materials* **2009**, *19*, 2187.
- (59) Wang, P.; Wenger, B.; Humphry-Baker, R.; Moser, J. E.; Teuscher, J.; Kantlehner, W.; Mezger, J.; Stoyanov, E. V.; Zakeeruddin, S. M.; Gratzel, M. *Journal of the American Chemical Society* **2005**, *127*, 6850.

- (60) Li, F.; Jennings, J. R.; Wang X.; Fan L.; Koh, Z. Y.; Yu, H.; Yan, L.; Wang, Q. *J. Phys. Chem. C* **2014**, *118*, 17153.
- (61) Hagberg, D. P.; Jiang, X.; Gabrielsson, E.; Linder, M.; Marinado, T.; Brinck, T.; Hagfeldt, A.; Sun, L. C. *J. Mater. Chem.* **2009**, *19*, 7232.
- (62) Idigoras, J.; Tena-Zaera, R.; Anta, J. A. *Physical Chemistry Chemical Physics*. **2014**, *16*, 21513.
- (63) Ivanistsev, V. a. F., M.V. *The Electrochemical Society Interface*. Spring 2014, 65.
- (64) Pazoki, M.; Boschloo, G.; Hagfeldt, A. *Electrochim Acta* **2015**.
- (65) Teuscher, J.; Marchioro, A.; Andrés, J.; Roch, L.M.; Xu, M.; Zakeeruddin, S.M.; Wang, P.; Grätzel, M.; Moser, J.E. *J. Phys. Chem. C* **2014**, *118*, 17108-17115.
- (66) Oskam, G.; Bergeron, B.V.; Meyer, G. J.; Searson, P.C. *J. Phys. Chem B*, **2001**, *105*, 6867-6873.
- (67) Dintcheva, N.; Furlani, M.; Jayasundara, W.; Bandara, T.; Mellander, B.-E.; Mantia, F. *Rheol. Acta* **2013**, *52*, 881-889

